

9. Conclusions

A 3D primitive equation model was applied to the TFZ to examine the hydrodynamics of the region. Using a nesting process to provide boundary conditions for the TFZ model, the region was represented with high resolution while incorporating forcing due to wind stress, tides, low frequency sea level oscillations and pressure gradients due to temperature and salinity distributions. The open boundaries of this model were supplied from a larger scale regional model that encompassed the whole of Spencer Gulf. This model was in turn forced with data collected in the field. The model was simulated for 12 months for the period Sep 2005 – Aug 2006 and calibrated to sea level measurements at Port Lincoln, Whyalla and Wallaroo, and temperature, salinity and velocity at numerous locations in the TFZ region obtained from a dedicated field program. The model was able to successfully reproduce tidal and low frequency sea level oscillations in both regional and TFZ models. Temperature, salinity and currents corresponding to tidal (diurnal) and weather band (periods 3-20 days) frequencies were also successfully reproduced by the model.

Both the data and model results showed there to be strong ($\sim 20 \text{ cm s}^{-1}$) tidal currents that may be implicated in bottom stirring. Although the tide may be responsible for trajectories of over 8 km, the net displacements due to these currents are small (less than 1.4 km over a 3 hr period). Magnitudes of the weather-band currents are smaller than the tidal currents ($< 5 \text{ cm s}^{-1}$), but due to their longer periods these currents are the dominant contributor to residual flow and hence primarily responsible for transport and flushing of the region. Both data and model indicate the residual currents eastward of Boston Island (in the tuna farming zone) to be weak ($\sim 1 \text{ cm s}^{-1}$) and to the north/north east during both summer and winter. The transport due to these flows over a 3-month period is around 80 km. The currents were also found to be strongly sheared in the vertical and so may be important to shear enhanced diffusion and dispersal. However, estimates of the flushing times based on tracers and Lagrangian tracking show flushing time-scales of 10 days (Boston Bay) to 2 days for the outer bay region. The flushing time for the whole domain based on particle tracking is ~ 20 days.

The tide in the region is classified as semi-diurnal mixed and is dominated by the semi-diurnal constituents M2 and S2, and the diurnal constituents K1 and O1. Coincidentally, all these constituents have approximately the same amplitude of $\sim 0.18 \text{ m}$, and when they are out of phase they destructively combine to produce very little tidal variation for several days. During these periods, called the 'dodge tide', the tidal currents are small and transport is primarily wind driven. If wind-speed is low, then it is possible that the region is very poorly flushed. The model was able to reproduce the occurrence of the dodge tide, allowing predictive capability of the timing of these events.

There exists a degree of connectivity between the coastal zone and the TFZ region in summer that can be caused by local upwelling. Offshore (eastward) winds force surface waters offshore, resulting in compensatory onshore interior or bottom flow. In addition, the larger evaporation that occurs near the coast leads to dense water formation and bottom plumes that flow to the outer bay region. During winter, similar plumes result from coastal cooling rather than evaporation. The annual temperature cycle in the TFZ region is largely driven by atmospheric heating and cooling. Salinity is also controlled by atmospheric exchanges, but to a lesser extent, with advective processes playing a dominant role. Large decreases in salinity in autumn occur, coincident with the flushing of Spencer Gulf when fresher compensatory

oceanic flows enter western Spencer Gulf. Due to the atmospheric exchanges, the TFZ was found to be stratified during summer and well mixed during winter.

The depth averaged seasonal flow can be divided into three main sub-regions within the domain. Firstly, offshore of Boston Island flow enters the domain in the south and exits in the north, with little penetration into the coastal margins. Secondly, the Boston Bay / Proper Bay area can be treated as a separate system, with flow generally entering north of Boston Island, flowing south to loop through Proper Bay and exiting to the east of Boston Island, where a persistent anti-clockwise gyre exists off Cape Donnington. Thirdly, Louth and Peake Bays exhibit northwards flow along the coast, fed by water seaward of Point Boston, and seasonally exhibiting gyres within Peake Bay and off Louth Island.

This residual flow determines the connectivity of the region, which consequently can be categorised into three main sub-regions, consistent with passive tracer and particle tracking analyses;

1. A region encompassing Proper Bay and the area landward of Boston Island, which has poor connectivity with the rest of the domain,
2. Louth and Peake Bay's, which also have poor connectivity with the rest of the domain,
3. Regions outside these bays and offshore of Boston Island with good connectivity with the remainder of the domain, but subject to greater flushing.

The TFZ numerical model was found to have satisfactory predictive skill, and as such is a suitable tool to couple to sediment transport and biogeochemical models to allow transport of nutrients/sediments etc through the model domain, and thus to provide a realistic spatial model of the dynamics of these substances.

10. References

- Atkinson I. et al (2004) Field report on the second survey of dry season water column and sediment properties in the Fitzroy Estuary and Keppel Bay, Rockhampton Queensland, August 15 – September 1, 2004. Coastal CRC, Contaminants dynamics sub-project. Milestones AC09, AC11, AC43 and AC44.
- Blanc, T.V. (1985) Variation of bulk-derived surface flux, stability, and roughness results due to the use of different transfer coefficient schemes. *J. Phys. Oceanogr.*, 15, 650-669.
- Blumberg, A.F. and Herring, J., (1987) Circulation modelling using orthogonal curvilinear coordinates, in *Three-Dimensional Models of marine and Estuarine Dynamics*, eds. Nihoul, J.C.J and Jamart, B.M., Elsevier.
- Blumberg, A.F. and L.H. Kantha (1985) Open boundary condition for circulation models, *J. Hydraulic Engineering*, 111, pp237-255.
- Eanes, R. and S. Bettadpur (1995) The CSR 3.0 global ocean tide model. *Center for Space Research, Technical Memorandum, CST-TM-95-06*.
- Easton, A. K. (1970). The tides of the continent of Australia. Horace Lamb Centre for Oceanographical Research, Res. Paper 37, Flinders University, South Australia.
- Easton, A. K. (1978). A Reappraisal of the Tides in Spencer Gulf, South Australia. *Aust. J. Mar. Freshw. Res.* 29, 467-477.
- Griffes, S.M., Hallberg, R. W., (2000) Biharmonic friction with a Smagorinsky viscosity for use in large-scale eddy-permitting ocean models. *Mon. Weath. Rev.*, 128, 2935-2946.
- Herzfeld, M. (2005) SHOC, sparse hydrodynamic ocean code, scientific manual. CSIRO Marine and Atmospheric Research.
- Herzfeld, M. (2006) An alternative coordinate system for solving finite difference ocean models. *Ocean Modelling*, 14, 174 – 196.
- Kitaigorodskii, S.A., O.A. Kuznetsov and G.N. Panin (1973) Coefficients of drag, sensible heat and evaporation in the atmosphere over the surface of the sea. *Izv. Acad. Sci. USSR Meteorology*, 9, 91-112.
- Kondo, J. (1975) Air-sea bulk transfer coefficients in diabatic conditions. *Boundary-Layer Meteorology*, 9, 91-112.
- Large, W.G., and S. Pond (1981) Open ocean momentum flux measurements in moderate to strong winds, *J. Phys. Oceanogr.*, 11, 324-336.
- Lennon, G.W., D.G. Bowers, R.A. Nunes, B.D. Scott, M. Ali, J. Boyle, C. Wenju, M. Herzfeld, G. Johansson, S. Nield, P. Petrushevics, P. Stephenson, A.A. Suskin and S.E.A. Wijffles (1987) Gravity currents and the release of salt from an inverse estuary. *Nature*, 327, 695-697.
- Leonard, B.P. (1979) A stable and accurate convective modelling procedure based on quadratic upstream interpolation. *Comp. Methods in Appl Mech. and Eng.*, 19, 59 – 98.
- Leonard, B.P. (1991) The ULTIMATE conservative difference scheme applied to unsteady one-dimensional advection. *Comp. Methods in Appl. Mech. and Eng.*, 19, 17 – 74.
- McClatchie, S., J.F. Middleton and T. Ward (2006) Water mass analysis and alongshore variation in upwelling intensity in the eastern Great Australian Bight. *J. Geophys. Res.*, 111, C08007, doi:10.1029/2004JC002699.
- Masagutov, T.F. (1981) Calculation of the vertical turbulent fluxes in the near-water atmospheric layer over the ocean in tropical latitudes. *Meteor. Hidrol.*, 12, 61-68.
- Mellor, G.L. and T. Yamada (1982) Development of a turbulence closure model for geophysical fluid problems. *Rev. Geophysics and Space Phys.*, 20(4), 851-875.
- Miller, M.J. and A.J. Thorpe (1981) Radiation conditions for the lateral boundaries of limited-area numerical models. *Q. J. R. Meteorol. Soc.*, 107, 615 - 628.

- Middleton, J. F., Platov, G. (2003). The Mean Summertime Circulation along Australia's Southern Shelves: a numerical study. *J. Phys. Oceanogr.*, 33(3), 2270-2287.
- Middleton J. F., Platov, G. (2005). Hydrodynamic model of the Great Australian Bight. Ward T., Goldsworthy S. D. and B. C. Page, Eds, In Tropho-dynamics of the GAB: Assessing the Need for an Ecological Allocation in the SA Pilchard Fishery. Report to the Fisheries Res. Develop. Corp., Proj. Number 2003/072, SARDI Aquatic Sciences Publication Number RD03/0166-2, pp 51-99.
- Middleton J. F., Arthur, C., van Ruth, P., Ward, T., McClean, J., Maltrud, M., Gill, P., Levings, A., Middleton, S. (2007). El Nino effects and upwelling off South Australia., *J. Phys. Oceanogr.*, 37, 2458-2477.
- Middleton, J.F, and C. Teixeira (2008) Wind-forced motion in Spencer Gulf: a numerical study. In preparation.
- Nixon, J. B., Noye, B. J. (1999). Prawn Larvae Advection-Diffusion Modelling in Spencer Gulf. In Noye, B.J., ed., Modelling Coastal Sea Processes, p189-218.
- Noye, B. J., Matthews, K., Grzechnik, M. P. (1999a). A three dimensional model of tides and surges in the Great Australian Bight. In Noye, B.J., Ed., Modelling Coastal Sea Processes, p107-134.
- Noye, B. J., Grzechnik, M., Stevens, J. M. (1999b). Modelling Currents and Dispersion in Boston Bay, South Australia. In Noye, B.J., ed., Modelling Coastal Sea Processes, 1, 247-272.
- Nunes Vaz, R.A., Lennon, G. W., Bowers, D. G. (1990). Physical Behaviour of a large inverse estuary. *Cont. Shelf Res.*, 10, 277-304.
- Nunes, R.A., Lennon, G. W., (1987). Episodic Stratification and Gravity Currents in a Marine Environment of Modulated Turbulence. *J. Geophys. Res.*, 92, 5465-5480.
- Petrusevics. P.M. (1993). SST fronts in inverse estuaries, South Australia – indicators of reduced gulf-shelf exchange. *Aust. J. Mar. Freshwater Res.* 44 305-323.
- Petkovic, P., Buchanan, C., (2002) January 2002 edition of the AGSO bathymetry. Geographic projection WGS84 Datum. Australian bathymetry and topography grid. Canberra: Geoscience Australia.
- Ridgway, K. J., Dunn, J., Griffin, D., Cahill, M., (2006) SynTS – a 3D ocean observational analysis for the Australian region, Second Argo Science Workshop, Venice, Italy.
- Ridgway K. R., J. R. Dunn and J. L. Wilkin (2002) Ocean interpolation by four-dimensional least squares -Application to the waters around Australia, *J. Atmos. Ocean. Tech.*, 19, 1357-1375.
- Simons, T.J., (1974) Verification of numerical models of lake Ontario. Part I, circulation in spring and early summer. *J. Phys. Oceanogr.*, 4, 507 – 523.
- Simpson, J.J. and T.D. Dickey (1981) The relationship between downward irradiance and upper ocean structure. *J. Phys. Oceanogr.*, 11, 309 - 323.
- Smagorinsky, J. (1963) General circulation experiments with the primitive equations, I. The basic experiment. *Mon. Wea. Rev.*, 91, 99 – 164.
- Smith, S.D., (1980) wind stress and heat flux over the ocean in gale force winds. *J. Phys. Oceanogr.*, 10, 709-726
- Tanner, J.E. & J.K. Volkman (2008) Aquafin CRC - Southern Bluefin Tuna Aquaculture Subprogram: Risk and Response – Understanding the Tuna Farming Environment. Technical report, Aquafin CRC Project 4.6, FRDC Project 2005/059. Aquafin CRC, Fisheries Research & Development Corporation and South Australian Research & Development Institute (Aquatic Sciences), Adelaide. SARDI Publication NoF2008/000646-1, SARDI Research Report Series No 344, 289 pp.

- Tartinville, B., E. Deleersnijder and J. Rancher (1997) The water residence time in the Mururoa atoll lagoon: sensitivity analysis of a three-dimensional model. *Coral Reefs*, 16, 193 – 203.
- Thompson, R.O.R.Y. (1983) Low-pass filters to suppress inertial and tidal frequencies. *J. Phys. Oceanogr.*, 13(6), 1077-1083.
- Walker, S.J. and J.R. Waring (1998) A multiple grid, 3-dimensional, non-linear, variable-density hydrodynamic model with curvilinear horizontal coordinates and level (z) vertical coordinates, CSIRO Marine Research, Report OMR-118/120.

11. Appendix A: A Re-Analysis of the Gulf Mouth Sea Level Data

11.1. Summary

The sea level records from M1 and M2 were found to have datum shifts of 10 – 20 cm brought about by re-deployment of the instruments at slightly different depths after servicing. Such datum shifts must be eliminated if the data is to be used to drive the model open boundary for periods longer than the minimum period of co-incident data (42 days). In addition, from the equipment available, the pressure sensors used on moorings M1 and M2 only gave estimates of sea level height to within a centimetre or so and no averaging was made to eliminate aliasing due to waves. Depths were recorded every 15 minutes. Mooring M3 did use a high quality tide gauge sensor and the 15 minute samples were obtained as burst (4 minute) averages. Thus, the quality of the M1 and M2 sea level data remains to be determined.

To this end a re-analysis is made of the low-passed filtered sea level data from the gulf sites M1 to M5. First, the low-pass filtered data at site M5 is found to be very similar to that at site M1 so that data from the former (M5) can be used to produce a long 10 month time series of continuous data at site M1. This also gives confidence in the M1 data collected. Similar continuous data sets are obtained for site M2 and M3. The seasonal sea level signal at M3 is assumed for sites M1 and M2 and the underlying assumption is that no net geostrophic flow into the gulf occurs for periods 2 months or greater. Using these long time series, a simple conceptual model is then developed to explain the net in/out flows into the gulf mouth that appear to be driven in part by the alongshore wind stress. The M1, M2 and M3 sea level data also suggests the existence of anticyclonic (cyclonic) circulation patterns near the gulf mouth and during periods of upwelling (downwelling) winds. These results are in qualitative agreement with recent numerical studies elsewhere (Middleton and Teixeira 2008).

With care, the M1, M2 and M3 time series will be used to drive the SHOC model.

11.2. The sea level data

A summary of the sea level data is given in Table 11.1. As shown in the first row, there are four coincident periods (42-68 days) when all M1, M2 and M3 data were obtained. The sub-records for these periods have been extracted, filtered to remove tides and then de-meanned. The results will be presented below. However, low-pass filtering loses 10 days per record and the result is that the final (gappy) sub-records are too short to be useful for driving the low-frequency circulation (3-20 day period) at the mouth of the gulf.

Here, we outline a re-analysis of the data so as to fill the gaps in the raw data, and derive three long time series at M1, M2 and M3 that might be useful in driving the model and in inferring the (low-frequency geostrophic) circulation near the gulf mouth.

11.3. Creation of long time series

To create the longest times series possible for each of the M1, M2 and M3 sites, the missing records were filled using the following procedure on the raw data files. First, each sub-series (Table 11.1) had the arithmetic means removed. The resultant data series were labelled rawmnd.dat where $m=1,2,3,4,5$ or 6 denotes the mooring site and $n=1,2,3$ or 4 the deployment period (see Table 11.2).

Table 11.1. Start and end times of mooring data. The first row lists the maximum coincident period for moorings 1, 2 and 3. The relevant start and finish times for the appropriate mooring are highlighted in bold. The last row lists the subsequent gaps between each of the maximum coincident periods in the first row. For M3, only two deployments were made and the data spans the periods indicated. These periods are indicated in days since 1990 that is adopted for the modelling. Some calendar dates are included.

Mooring	Deployment 1 68 days Sept-Oct		Deployment 2 63 days Dec-Jan		Deployment 3 42 days March-April		Deployment 4 55days May-June OR 79 days May-July	
	start	end	start	end	start	end	start	end
M1	5720.5	5790.25 – Nov 8	5812.375	5918.25	5918.5 - March 16	5981.5	5981.75 May 18	6066.37
M2	5722.62 - aug30			5875.375 – Feb 1	5875.625	5974.45 May 11	5987.625 –May 24	6085.5
M3	5722.37			5888.5 48 Feb 14	5888.75 March 14			6070.25
M4	5721.5	5793			5887.5	5963	5981.625	6050.37
M5	5720.5	5792	5799.5	5878	5887.5	5960.625	5981.5	6045
M6							5981.75	6042.37
		22 day gap		43 day gap		17 day gap		

Table 11.2. Means (cm) of raw, filtered and filtered & trimmed data sub-series for deployments d1, d2, d3, d4. A dash means no data for that period. Documentation for the calculation of the means indicted by the ^ have not been located.

Data file	Mean deploy 1	Mean deploy 2	Mean deploy 3	Mean deploy 4
rawm1d*	441.1	407.6	420.92	477.2
fm1d*	440.3	406.7	421.6	477.5
fm1s*	440.4	409.5	418.8	477.5
rawm2d*	-----	0.000^	537.96	540.15
fm2d*	-----	0.85^	537.85	540.21
fm2s*				
rawm3d*	-----	4833.0	-----	4847.7
fm3d*	-----	4833.3	-----	4847.0
fm3s*				
rawm4d*	1380.1	-----	965.5	903.8
fm4d*	1379.7	-----	965.0	905.0
fm4s*	1379.8	-----	970.1	904.7
rawm5d*	1853.5	1989.2	2005.3	2013.4
fm5d*	1852.9	1990.6	2005.9	2015.0
fm5s*	1853.2	1992.6	2010.0	2015.0

Subtraction of the means is necessary due to the arbitrary datum shifts (water depths) that arose after servicing and redeployment. From Table 11.2, these can be large (~10-40 cm) and without correction will drive significant and erroneous geostrophic currents. Note, the datum shifts can also arise from seasonal and intra-seasonal (ENSO) influences.

Filling the Gaps:

Site M1: This site has the most and longest gaps. Based on the observation below that the M5 and M1 low pass filtered data are almost identical for the August - December 2005 period, the M5 data was used from deployment periods 1 & 2 to cover the period 5720.50 to 5812.33. There is a 7.5 day gap between these two records from 5792.04 to 5799.00. This was filled with data from site 2 so that the net geostrophic flow into the gulf is implied to be zero for this period.

After time 5812.33, the raw data from site 1 was used and the remaining $\frac{1}{4}$ day gaps filled using the hourly data from the following or preceding day.

Site M2: The first two deployment files were added and the $\frac{1}{3}$ day gap interpolated using the following $\frac{1}{4}$ day of data. A 13 day gap between this file and the next file was interpolated using 13 days of data from site 1. The net geostrophic flow thru the gulf mouth is therefore zero over this time (11-24th May 2006).

Site M3: This site has only a $\frac{1}{4}$ day gap that was filled using hourly values from the following day's time series.

The process above ensures that the time series at each site are continuous (days 5720.50 to 6042.37) and the datum shifts are eliminated: the cost of elimination is that each of the sub-records used to obtain the continuous series have zero mean and thus the implied net geostrophic flow (proportional to the sea level difference) into the gulf is necessarily zero (2 months or longer).

The resultant continuous series were called rawm1.dat, rawm2.dat etc. These were then filtered using the Thompson (1984) low pass filter (cut-off 29hrs). The filter results in a loss of 5 days of data at each end of the time series. These three series were then trimmed so that all start at 5725.500 and end at 6061.375 and given the labels fmklong.dat where k=1,2 or 3 denotes the site.

Figures 11.1, 11.2 and 11.3 contain the long filtered time series for sites 1, 2 and 3 along with the short (original) filtered records. The mean of each sub-series is set to zero as is the mean of the long records. As can be seen, the long and short records generally differ by some constant suggesting that seasonal or intra-seasonal effects are important.

Seasonal Effects:

To determine these, we have calculated a running 2-month average of the long time series (Figure 11.4). As is evident, the seasonal variability indicated is much larger at M3 than either M1 or M2. This is thought to be due to the number of sub-records used to determine each long time series. For M3, only 2 sub-records were used and each was around 5 months in length. For M1 and M2, 4 records were used and for each the sub-record the mean was subtracted (and thus part of the seasonal trend).

In Figure 11.5 we present the 3-month averaged sea level from sites between Victor Harbour and Thevenard as obtained by Middleton et al (2007). Clearly there is a great deal of variability at the seasonal and intra-seasonal time scales. Middleton et al (2008) have averaged the monthly averaged data from Outer Harbour and Thevenard to obtain the seasonal signal shown in Figure 11.6. It has a maximum amplitude of only 3 cm and much less than the 2005-2006 value from M3 which is about 10 cm. The reason for the difference may be in part due to the El Nino effects which will act to lower sea level at all sites by the same amount. Plotted along with the sea level is the $-nino3.4$ index which when negative (positive) indicates El Nino (La Nina) conditions. It is evidently correlated with the sea level signals, and for 1998-1999 the El Nino signal in sea level was about 7 cm.

Readjusting the Data:

The differences in the seasonal values of sea level at sites 1, 2 and 3 are thought to be due to the subtraction of the means for each component sub-series used. Since M3 has the best sea level sensor and least sub-records, we will adopt its 2-month running mean for both M1 and M2. This is simply done by subtraction of the means shown in Figure 11.4 from the long time series and then by the addition of the 2-month running mean for M3. The underlying assumption is then that there is no net geostrophic flow into gulf at periods of 2 months or more.

The resultant readjusted filtered/trimmed long records are shown in Figure 11.7. We next investigate the reliability or otherwise of these records.

11.4 Geostrophic Currents

To investigate this we have determined the net geostrophic velocity (v_{12}) into the gulf mouth using the difference in sea level between sites 1 and 2. The results are presented in Figure 11.8 along with Ekman velocity computed from the Neptune Island wind stress and off-set by -20 cm s^{-1} for clarity. An average water depth of 20 m is assumed. Note that both velocities have been further filtered using a 3-day running block-average to mask the large 2-3 day variability.

Notably, the positive geostrophic velocities (into the gulf) are inversely correlated with the negative Ekman velocities (out of the gulf). This inverse correlation is consistent with a simple geostrophic model shown in Figure 11.9. For the upwelling favourable winds shown, the surface (out of gulf) Ekman transport must be largely offset by an into gulf geostrophic velocity. This geostrophic velocity must be accompanied by a relative high on the western side of the gulf (as indicated by the H). For downwelling favourable winds, the reverse holds and the model is crudely consistent with the observations in Figure 11.8.

Note, in this simple model, we ignore effects that arise from the onshore winds, density and friction in the bottom boundary.

In addition, we note that when the winds relax, that the sea level difference across the gulf mouth may vanish and the alongshore flow bends into the gulf mouth as shown in Figure 11.10.

Now let us examine the geostrophic velocities between M1 and M3 (v_{13}) and M3 and M2 (v_{32}) shown in Figure 11.11 and 11.12. In Figure 11.12, a 3-day running average has been

applied to mask out the large 2-day variability and the alongshore wind stress is also shown. The geostrophic velocities here (Figure 11.12) are remarkably much larger ($\sim 20 \text{ cm s}^{-1}$) than the net between M1 and M2 ($\sim 5 \text{ cm s}^{-1}$) and largely self-compensating. That is, when there is a large flow into the gulf between M1 and M3, there is also a large flow out of the gulf between M3 and M2.

In addition, when the winds are upwelling favourable (days 5790-5810 & 5850-5920), there is an inflow between M1 and M3 (western side) and an outflow between M3 and M2 (eastern side). This flow suggests an anticyclonic circulation for upwelling conditions at the gulf mouth, such that the net transport may be largely set by the Ekman Transport. The reverse holds during downwelling winds.

The conceptual model above is supported by the numerical studies of Middleton and Teixeira (2008) who have examined the gulf response to idealized forcing by oscillatory winds. We conclude that the long, filtered time series may be indicative of true sea level although the variations in seasonal effects suggest they be used with care. In addition, the adjusted long time series for M1, M2 and M3 have been filtered using the Thompson filter (cut-of 29 hrs), but still contain much of the 2-3 day variability that is apparent in all the sea level records and wind stress. This adjusted data may need to be further filtered in line with other filtered data (wind stress) used to force the SCHOC model. In addition, the seasonal means were artificially set to the first (and last) constant value for M3 over the first 30 (and last 30 days) shown in Figure 11.8 (lower panel). Thus, the model results over these times may be suspect.

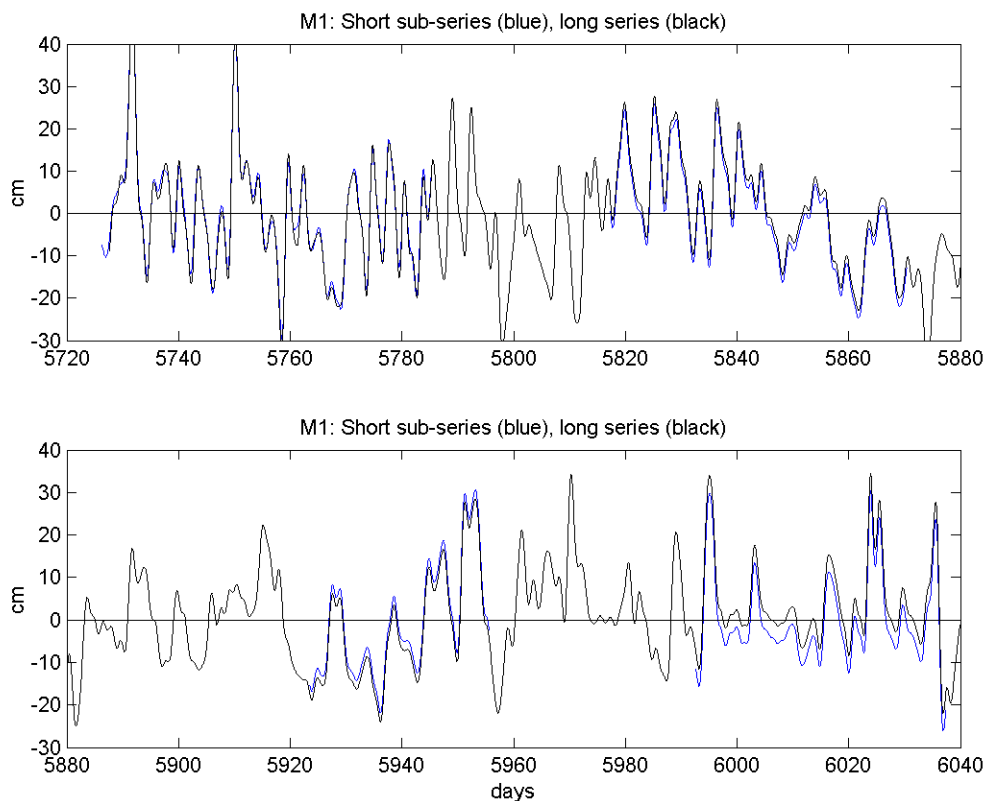


Figure 11.1. The long (black) and short (blue) sea level series for M1. Each long and short time series has zero mean.

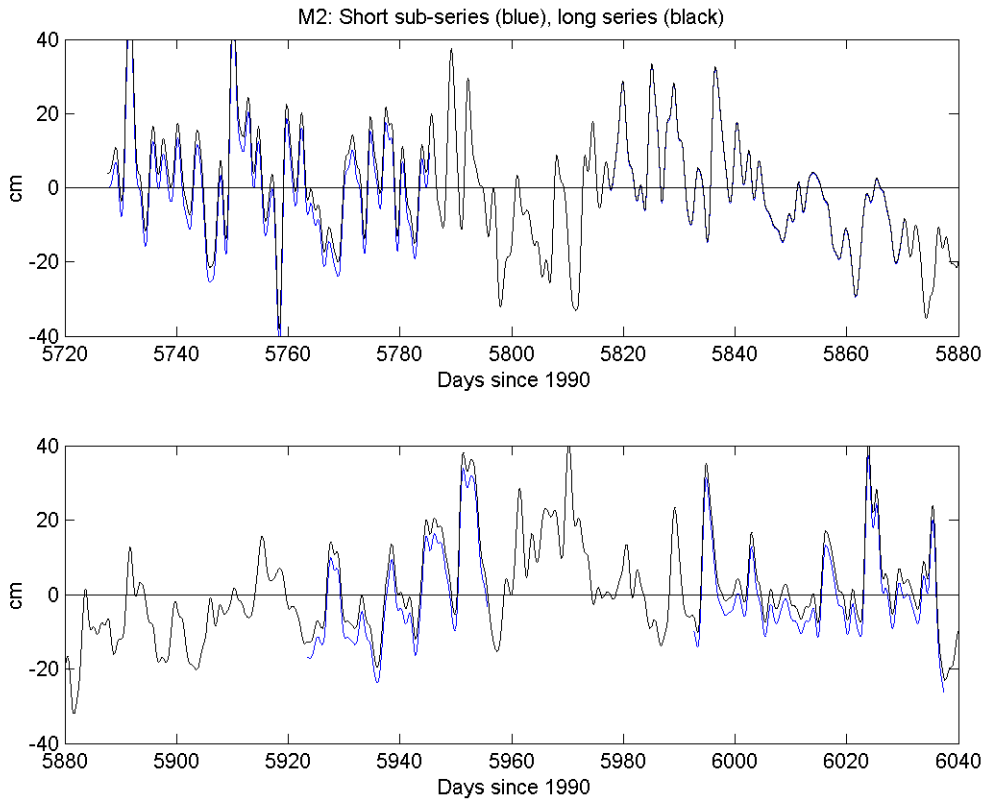


Figure 11.2. The long (black) and short (blue) sea level series for M2. Each long and short time series has zero mean. The long and short series are indistinguishable between days 5820 and 5880.

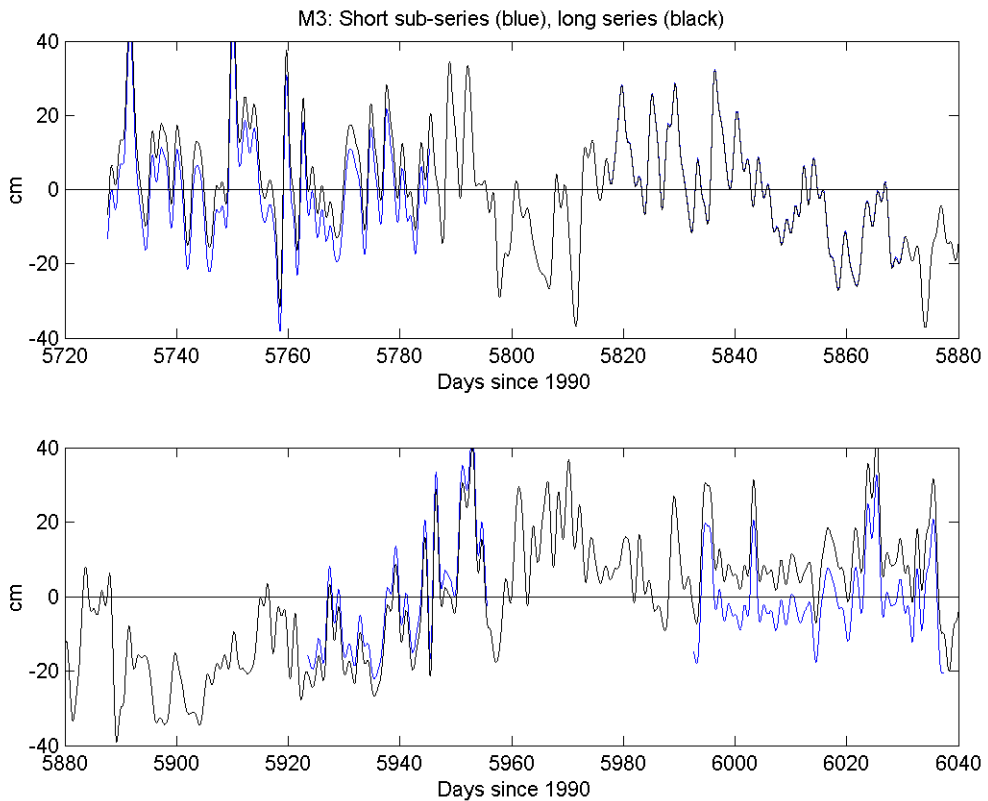


Figure 11.3. The long (black) and short (blue) sea level series for M3. Each long and short time series has zero mean. The long and short series are indistinguishable between days 5820 and 5880.

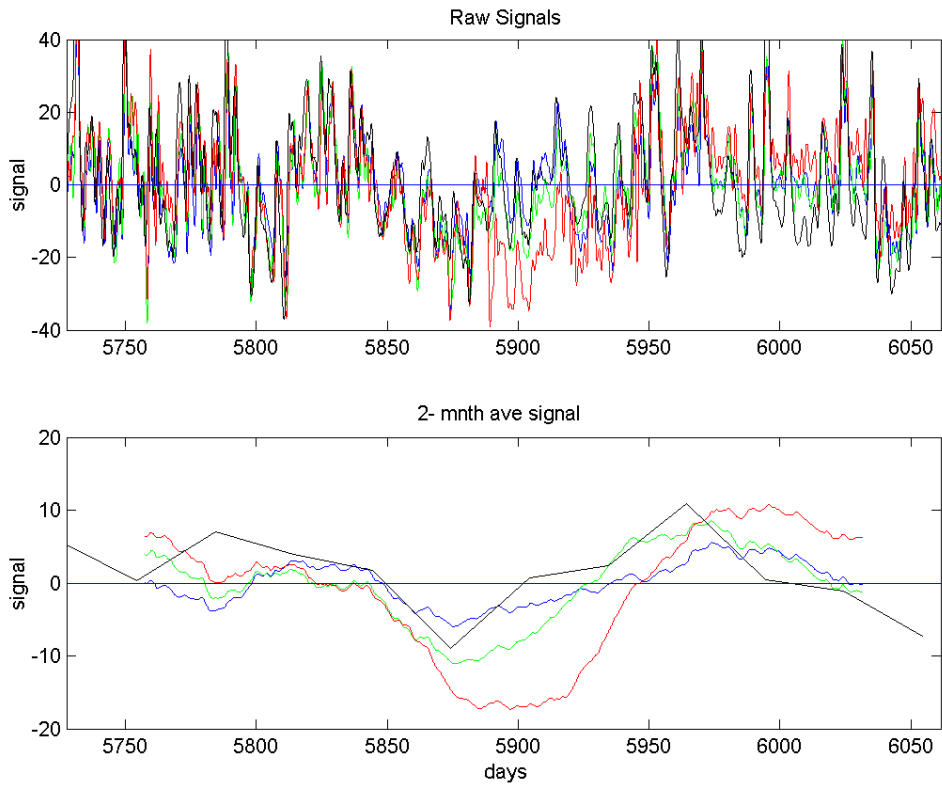


Figure 11.4. Upper: the (29hr-cut-off) Thompson filtered long sea level series. Lower: the 3-month average of the sea level data in the upper panel. The series are for M1 (blue), M2 (green), M3 (red) and Thevenard (black).

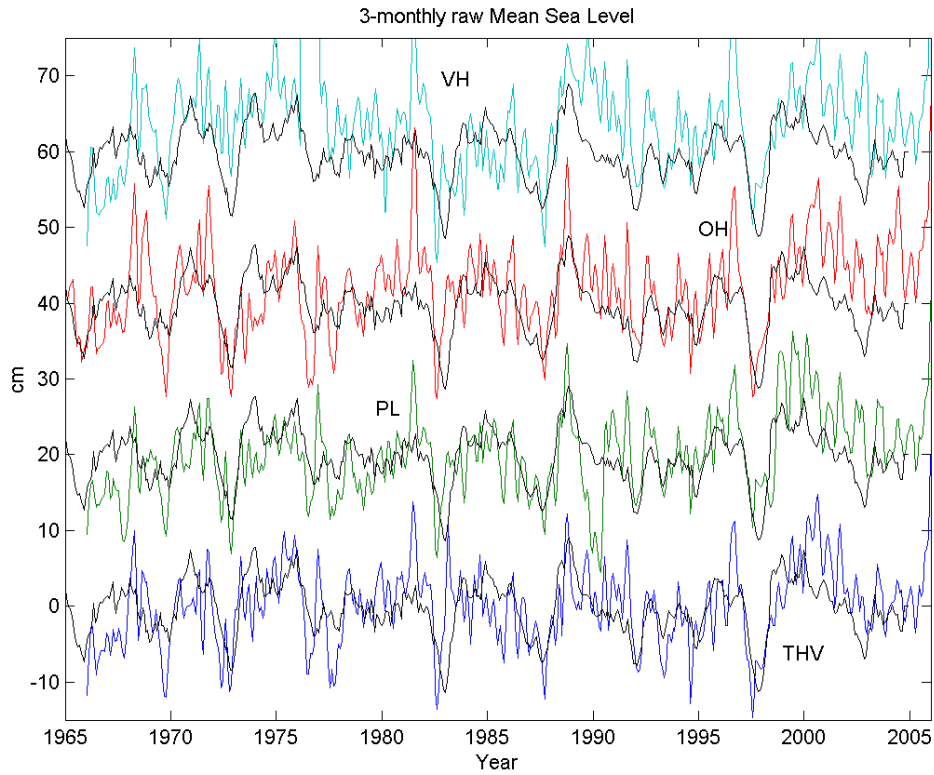


Figure 11.5. The 3-monthly averaged sea level from Thevenard (THV), Port Lincoln (PL), Outer Harbour (OH) and Victor Harbour (VH) offset by 20 m. The black curve is the $-nino3.4$ index which if negative indicates El Nino conditions.

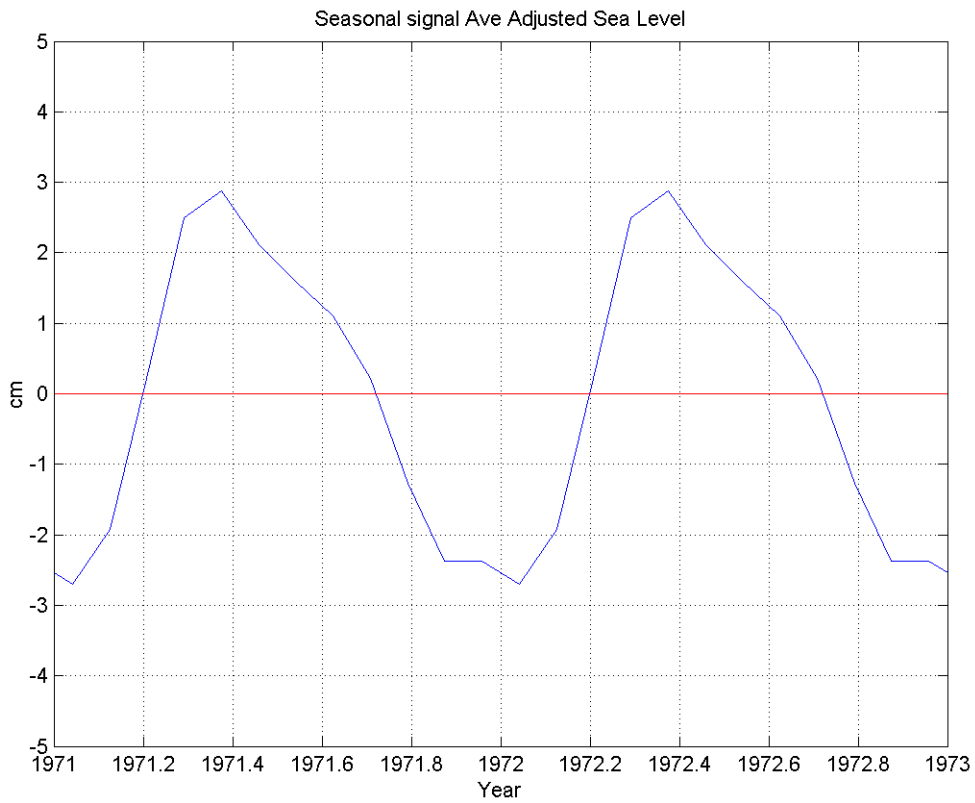


Figure 11.6 The monthly average of Thevenard and Outer Harbour sea level data for the 1971-1973 period. Note: the averages at the two sites were nearly identical, (from Middleton et al 2007).

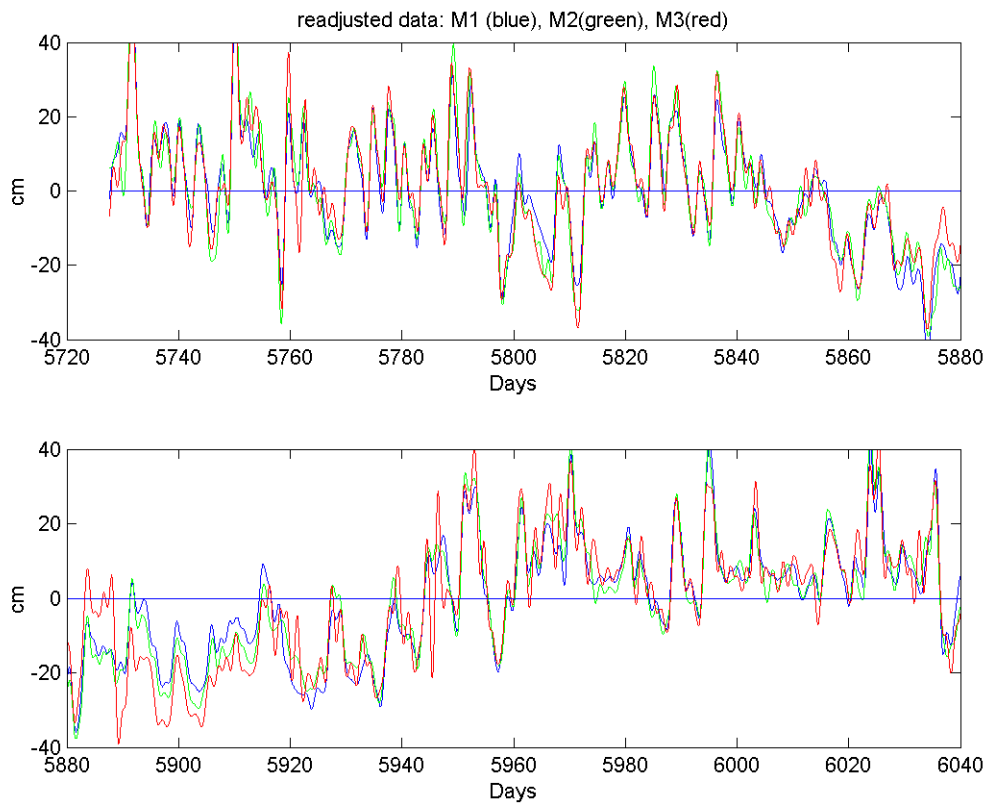


Figure 11.7. The long time series of sea-level data readjusted to all have the M3 seasonal (2-monthly) average shown in Figure 11.4.

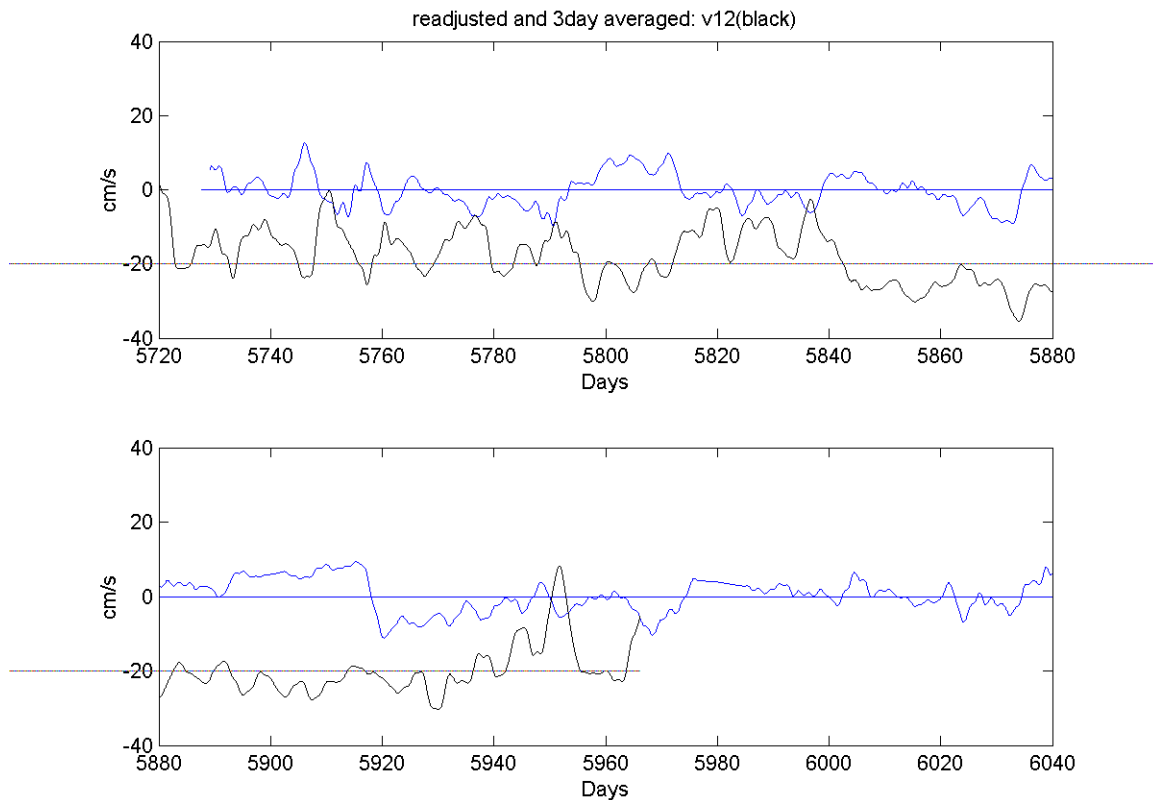


Figure 11.8 The geostrophic velocity v_{12} (blue) based on the M1 and M2 adjusted time series shown in Figure 11.7. Positive values are directed into the gulf. The black curve denotes the Ekman velocity driven by the wind stress (Neptune Island data). The Ekman velocities are offset by -20 cm s^{-1} and values below -20 are out of gulf while values above -20 are directed into the gulf. All data has been filtered using a 3-day running block average to eliminate the 2-day variability.

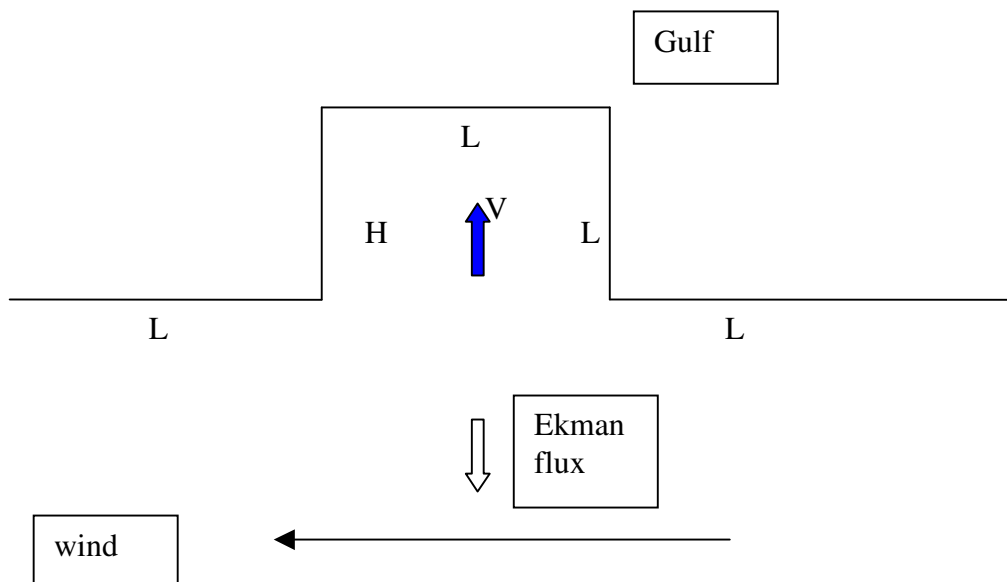


Figure 11.9. Schematic illustrating the northward geostrophic velocity v_{12} that should arise to offset the mass lost through the surface (out of gulf) Ekman transport for upwelling favourable winds. The geostrophic velocity must be accompanied by a relative high on the west gulf coast.

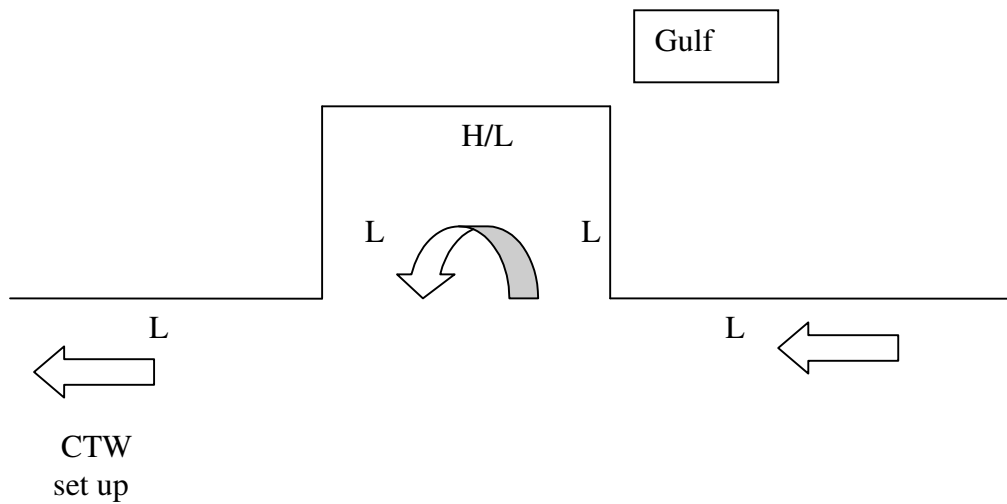


Figure 11.10. Schematic illustrating the shelf and gulf currents when no wind is present and the circulation is driven by coastal trapped waves (CTW) from the west. At the head of gulf, the currents are weak, while at the mouth, the currents lop into the gulf as shown.

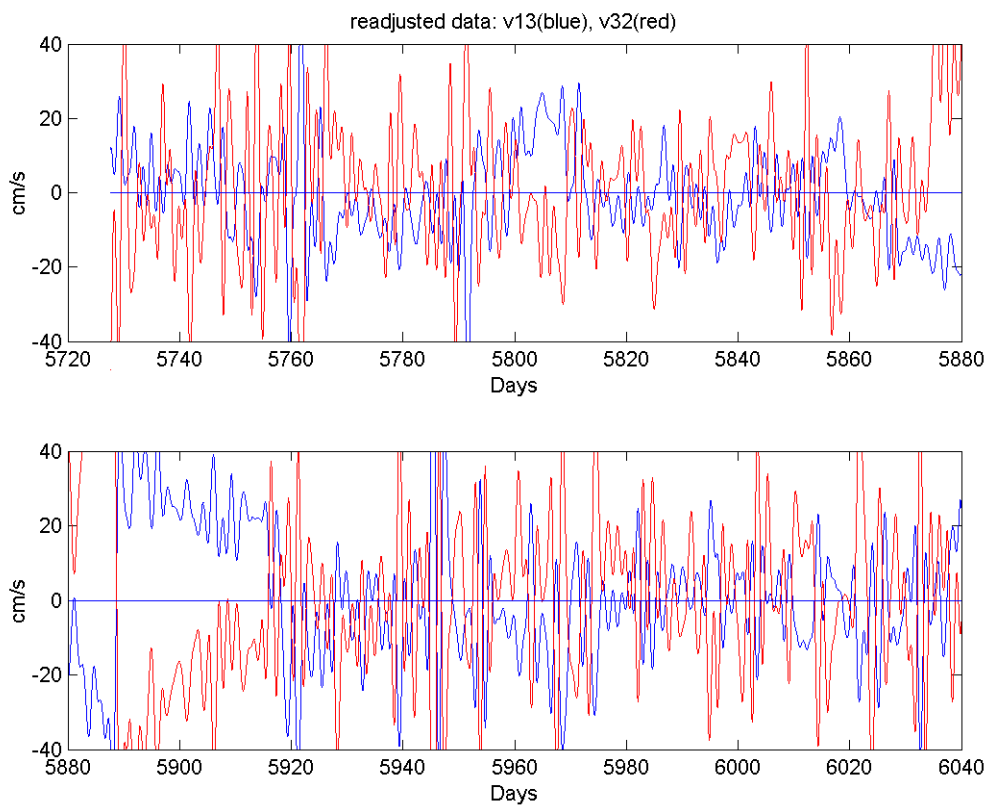


Figure 11.11. The geostrophic velocities v_{13} , and v_{32} based on the seasonally adjusted long times series for M1, M2, M3. Positive values are to the north (into gulf).

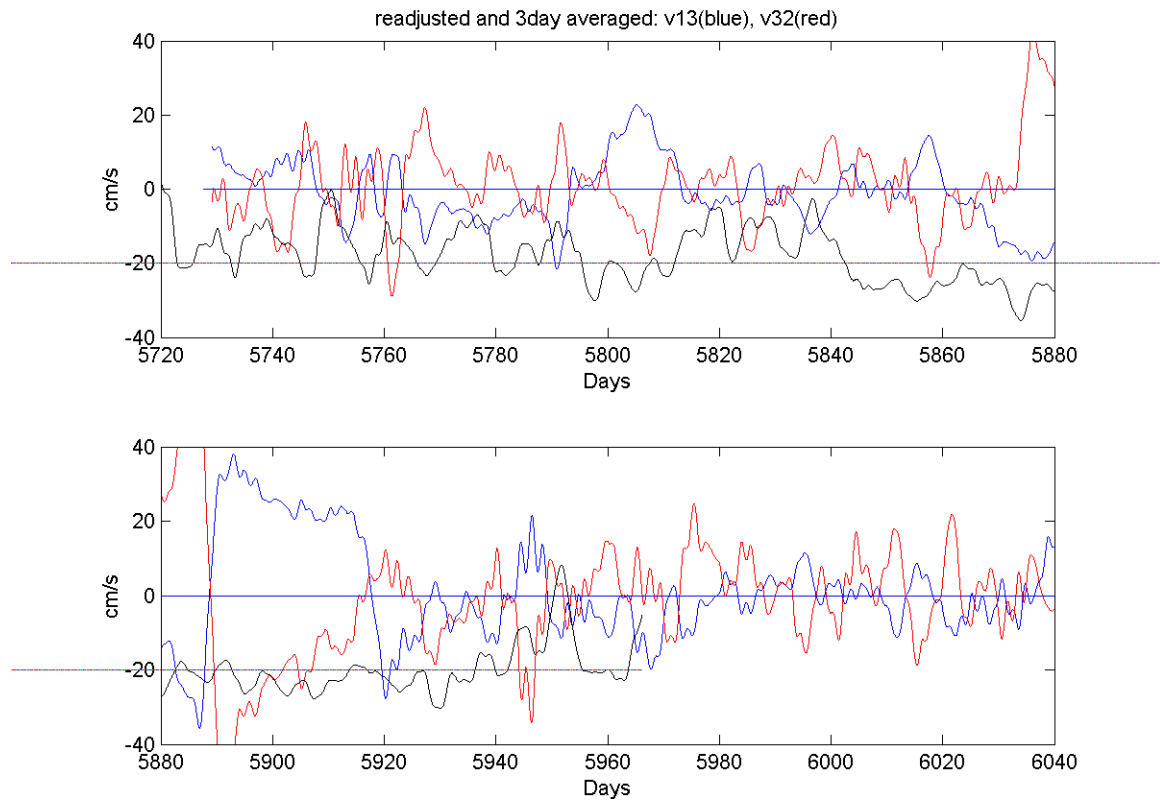


Figure 11.12. The geostrophic velocities v_{13} , and v_{32} based on the seasonally adjusted long times series for M1, M2, M3. Positive values are to the north (into gulf). A 3-day filter has been applied using a running block average to eliminate the 2-day variability.

12. Appendix B: Local Heating – a simple model

The contribution of local heating was considered using the air-sea heat flux computation in the SHOC. The model domain included all of Spencer Gulf with a detailed nested region in the vicinity of the tuna farming zone. The heat flux data output from the model was used to predict an incremental change in temperature δT over each day and for a mixed layer of depth H according to:

$$\delta T = \frac{tQ_f}{\rho_w C_p H}$$

where t = time increment (s),

Q_f = heat flux from model (Watts m^{-2}),

ρ_w = water density (1024 kg m^{-3}),

C_p = specific heat of water ($4000 \text{ J kg}^{-1} \text{ }^\circ\text{K}^{-1}$)

and H = depth (20 m).

13. Appendix C: Velocity shear

In general tidal currents are subject to bottom boundary layer shear, and wind-driven currents contain shear primarily in the surface layer. Shear can take the form of differences in both magnitude and direction due to rotational effects. We start by considering magnitude differences. Statistics for low pass filtered data (29 hour cutoff) and the tidal band are presented (as before, the tidal band data is formed by subtracting the low-filtered data from the unfiltered data). Since only M4 was able to resolve both surface and bottom boundary layers, we consider it first.

Surface and Bottom Shear - M4 Statistics

The following quantities are plotted in Figure 13.1: a) $s(t) - \bar{s}(t)$: “shear”, where $s(t)$ is the velocity magnitude in either the surface or bottom layer (plotted in red and blue respectively), and $\bar{s}(t)$ is the depth-mean of $s(t)$. b) $|s(t) - \bar{s}(t)|$: “shear magnitude”.

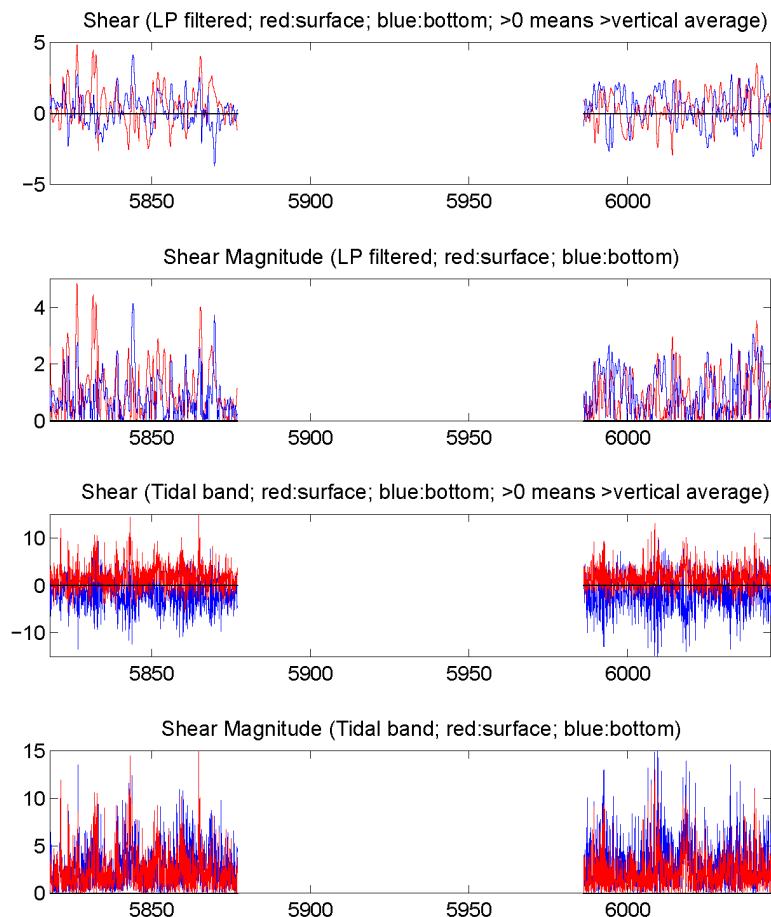


Figure 13.1. Difference between surface (and bottom) speed and that of the water column as a whole at Mooring 4. Low-frequency band (upper two panels) and tidal band (lower two panels). Red: surface minus depth-mean. Blue: bottom minus depth-mean. “Shear magnitude” is the absolute value of the difference.

The mean and rms of the difference time series of Figure 13.1 are given in Table 13.1. Units are cm s^{-1} . A positive/ negative value implies the boundary layer is faster/slower the mean.

Table 13.1. statistics of difference time series at Mooring 4

	Deployment 2 (summer)				Deployment 4 (winter)			
	Low Frequency		Tidal Band		Low Frequency		Tidal Band	
	mean	rms	mean	rms	mean	rms	mean	rms
surface	0.6	1.1	1.7	2.4	0.3	0.9	1.6	2.2
bottom	0.2	0.9	-1.6	2.7	0.4	1.1	-1.9	3.1

The surface and bottom velocity differences are both about three times higher in the tidal band than in the low-pass filtered band. In the tidal band the rms difference at the bottom is slightly higher than at the surface. In the low-pass filtered band, the bottom and surface shears are nearly equal.

The directions of the depth-mean current, and the surface and bottom deflections (both in degrees), for M4 are shown in Table 13.2. Positive (negative) deflections are measured counter-clockwise (clockwise) from the direction of the mean flow. The mean flow direction is the angle measured from east.

Table 13.2. Directions of flow at Mooring 4

	Deployment 2 (summer)		Deployment 4 (winter)	
	Low Frequency	Tidal Band	Low Frequency	Tidal Band
	depth-mean	47.0 ¹	84.8 ²	60.7 ¹
surface deflection	17.4	3.7	20.4	0.08
bottom deflection	-27.2	-8.5 ³	-29.8	-6.3 ³

1: The mean (over time) directions of the components (depth-average, surface, and bottom) are taken first, then the deflection angles (surface versus depth-mean, and bottom versus depth-mean) found.

2: For the tidal band only, the principal axis direction is used to define the mean flow direction.

3: Time mean of hourly deflections.

Shear Statistics for M4 and M5

Selected statistics for the current meters at M4 and M5 are summarized in the tables below, beginning with definitions of the values. The velocity units are cm s^{-1} .

Statistics for unfiltered, low pass filtered (29 hour cutoff), and the tidal band are presented (the tidal band is formed by subtracting the low-filtered data from the unfiltered data).

u, v : east-west and north-south components of velocity;

\bar{u}, \bar{v} : depth-integrated values of u, v ;

$u_{\text{rms}} = \sqrt{\langle \bar{u}^2 \rangle}$ (and similarly for v component): rms value of depth-mean currents (brackets indicate time average);

$$\sigma_z''(t) = \sqrt{\frac{1}{h} \int_{-h}^0 (u - \bar{u})^2 dz}$$

(and similarly for v component): standard deviation of the u component along the z (depth) axis; and

$\langle \sigma_z^u(t) \rangle$: time average of $\sigma_z^u(t)$ (and similarly for v component).

Mooring 4

Deployment 1: 29 August – 14 November 2005

Deployment 2: 16 November 2005 – 10 February 2006

Deployment 3: 11 February – 15 May 2006

Deployment 4: 15 May – 15 August 2006

Table 13.3. $\langle \bar{u} \rangle, \langle \bar{v} \rangle$: time averages of depth-mean current components at M4

D	Unfiltered				Low Frequency				Tidal Band			
	1	2	3	4	1	2	3	4	1	2	3	4
u	0.0	0.7	1.1	0.9	-0.1	0.7	1.1	0.9	0.0	0.0	0.0	0.0
v	0.7	0.6	0.7	1.8	0.6	0.6	0.7	1.8	0.0	0.0	0.0	0.0

D: Deployment; u and v in cm/s

Table 13.4. As in Table 13.3, taken over all deployments

	Unfiltered	Low Frequency	Tidal Band
u	0.7	0.7	0.0
v	0.9	0.9	0.0

Table 13.5. $\langle \sigma_z^u(t) \rangle, \langle \sigma_z^v(t) \rangle$: time averages of std. deviations along z-axis at M4

D	Unfiltered				Low Frequency				Tidal Band			
	1	2	3	4	1	2	3	4	1	2	3	4
u	5.0	21.7	7.1	10.6	1.7	2.6	3.4	3.9	4.2	4.9	5.9	3.8
v	11.3	37.6	11.1	23.7	1.6	1.3	1.4	1.8	14.6	13.8	16.3	10.9

D: Deployment; u and v in cm/s

Table 13.6. As in Table 13.5, taken over all deployments

	Unfiltered	Low Frequency	Tidal Band
u	11.1	2.9	4.7
v	20.9	1.5	13.9

Table 13.7. $\sqrt{\langle \bar{u}^2 \rangle}$, $\sqrt{\langle \bar{v}^2 \rangle}$: rms of depth-mean velocity components at M4

	Unfiltered				Low Frequency				Tidal Band			
	D	1	2	3	4	1	2	3	4	1	2	3
u	3.3	3.1	3.7	3.4	1.4	1.8	2.0	1.7	2.9	2.5	3.1	3.0
v	10.8	10.0	10.9	12.7	1.7	1.5	1.4	2.6	10.7	9.9	10.8	12.4

D: Deployment; u and v in cm/s

Table 13.8. As in Table 13.7, taken over all deployments

	Unfiltered	Low Frequency	Tidal Band
u	3.4	1.7	2.8
v	11.1	1.8	11.0

Mooring 5

Deployment 1: 30 August – 14 November 2005

Deployment 2: 16 November 2005 – 10 February 2006

Deployment 3: 11 February – 15 May 2006

Deployment 4: 16 May – 15 August 2006

Table 13.9. $\langle \bar{u} \rangle$, $\langle \bar{v} \rangle$: time averages of depth-mean current components at M5

	Unfiltered				Low Frequency				Tidal Band			
	D	1	2	3	4	1	2	3	4	1	2	3
u	-2.4	2.9	-	-1.6	-2.4	2.9	-	0.9	0.0	0.0	-	0.0
v	0.4	-4.0	-	0.8	0.4	-4.0	-	1.8	0.0	0.0	-	0.0

D: Deployment; u and v in cm/s

Table 13.10. As in Table 13.9, taken over all deployments

	Unfiltered	Low Frequency	Tidal Band
u	-0.4	-0.4	0.0
v	-0.9	-0.9	0.0

Table 13.11. $\langle \sigma_z^u(t) \rangle$, $\langle \sigma_z^v(t) \rangle$: time averages of std. deviations along z-axis at M5

	Unfiltered				Low Frequency				Tidal Band			
	D	1	2	3	4	1	2	3	4	1	2	3
u	2.2	3.8	-	5.5	1.3	1.8	-	1.9	3.3	3.7	-	3.4
v	3.9	3.9	-	5.2	2.0	1.2	-	3.9	5.9	2.3	-	3.0

D: Deployment; u and v in cm/s

Table 13.12. As in Table 13.11, taken over all deployments

	Unfiltered	Low Frequency	Tidal Band
u	3.9	1.7	3.4
v	4.3	2.3	3.7

Table 13.13. $\sqrt{\langle \bar{u}^2 \rangle}$, $\sqrt{\langle \bar{v}^2 \rangle}$: rms of depth-mean velocity components at M5

D	Unfiltered				Low Pass Filtered				Tidal Band			
	1	2	3	4	1	2	3	4	1	2	3	4
u	3.7	5.4	-	4.6	2.7	3.3	-	2.1	2.4	4.2	-	4.0
v	5.9	5.4	-	3.5	1.6	4.4	-	1.6	5.5	3.2	-	3.0

D: Deployment; u and v in cm/s

Table 13.14. As in Table 13.13, taken over all deployments at M5

	Raw	Low Frequency (subtidal)	Tidal Band
u	4.5	2.7	3.5
v	4.9	2.5	3.9